Atom Indonesia

Journal homepage: http://aij.batan.go.id

High Temperature Oxidation Behavior of Fe-Cr Steel in Air at 1000-1200 K

T. Sudiro*, D. Aryanto, A.S. Wismogroho, Ciswandi, B. Hermanto, H. Izzuddin and R. Pratama

Research Center for Physics, Indonesian Institute of Sciences, Puspiptek Area, Serpong, Tangerang Selatan 15310, Indonesia

ARTICLE INFO

Article history:
Received 9 February 2017
Received in revised form 4 November 2017
Accepted 8 November 2017

Keywords:
Fe-Cr steel
Oxidation kinetic
Breakaway
Phase
Microstructure

ABSTRACT

The high temperature oxidation behavior of Fe-Cr steel was studied in air at elevated temperatures of 1000, 1100 and 1200 K for up to 72 ks. The mass change of all samples was recorded in order to evaluate their oxidation kinetic. The structure of oxide scales was investigated by mean of X-ray diffraction and SEM-EDX. According to oxidation kinetic curve, the mass gain of oxidized sample increases with increasing oxidation time and temperature. At 1000 and 1100 K, the Fe-Cr steel exhibits an excellent oxidation resistance. As oxidation temperature increase to 1200 K, however, the accelerated oxidation occurred. This is considered due to breakaway oxidation. The Fe-Cr steel forms a duplex oxide layer consisting of Fe-rich oxides in the outer layer and Fe-Cr oxides in the inner layer. The obtained results suggest that the oxidation temperature strongly affects the oxidation resistance of Fe-Cr steel and the structure of formed oxide layer on the steel surface. The influence of oxidation temperature on the oxidation resistance and scale structure is discussed in this paper.

© 2018 Atom Indonesia. All rights reserved

INTRODUCTION

Fe-Cr steel has been widely used for power generating applications as boiler and metallic interconnect of solid oxide fuel cell (SOFC). When the steels are exposed to high temperature and oxidizing atmosphere, it forms oxide scale on their surface. It is well known that iron and alloyed steel usually form three oxides layer consisting of Fe_2O_3 in the outer layer, FeO on the steel surface and Fe_3O_4 at the Fe_2O_3/FeO interface [1-3] or two oxides layer consisting of Fe_3O_4 inner layer and Fe_2O_3 outer layer, depending on exposure temperature [2,3]. Meanwhile, the ferritic, martensitic and austenitic steels protection against oxidation and corrosion at high temperature are attributed to the formation of a protective Cr_2O_3 scale through selective oxidation of chromium [4-8]. Accordingly, the sufficient amount of Cr content is needed in order to maintain the oxide protectiveness at high temperature and avoid catastrophic failure of the steel.

During their service period, however, the degradation of protective oxide to non-protective oxide scale is liable to occur. This phenomenon is often namely as breakaway oxidation. Initially, the alloy forms a protective chromia oxide on the steel surface. Nevertheless, due to a mechanical damage or insufficient amount of Cr content in the alloy, further later on the protective chromia oxide transforms into unprotective oxide scale by forming Fe-rich oxides on the steel surface [6,8-10]. The degradation of chromia oxide can be caused by vaporization of the oxide by forming a volatile species of CrO_3 or $CrO_2(OH)_2$, especially at high temperature and wet atmosphere [8,9,11-13]. In addition, defects on the oxide scales as cracks and pores can enhance the anion diffusion to the substrate. Accordingly, the understanding of effect of Cr content, oxidation temperature and atmosphere on high temperature oxidation resistance of steels becomes particularly important.

*Corresponding author.
E-mail address: toto011@lipi.go.id
DOI: https://doi.org/10.17146/aij.2018.608

This study aims to clarify the effect of temperature on the resistance of Fe-Cr steel against oxidation at high temperature and scale structure developed on the steel surface. The X-ray diffraction and SEM-EDX were used to investigate the phase composition and scale structure of the sample after high temperature oxidation at 1000, 1100 and 1200 K.

EXPERIMENTAL METHODS

Sample preparation

The commercial available of Fe-Cr steel with a nominal composition of balance Fe, 16 wt. % Cr, 0.29 wt. % Mn, 0.25 wt. % Si, small concentration of C, P and S was used in this study. The specimens for high temperature oxidation test were cut from Fe-Cr steel sheet into dimension of about 1.5 × 1.5 × 0.2 mm. Before high temperature oxidation test, the samples were ultrasonically degreased in ethanol solution and weighted using electronic balances (Precision: 0.01 mg) for oxidation kinetic evaluation.

High temperature oxidation test

The high temperature oxidation test was performed in a muffle furnace. The specimen was exposedin air at elevated temperature of 1000, 1100 and 1200 K, separately. Firstly, the furnace was heated from room temperature to the aforesaid temperatures. After the desired temperature was reached, the specimen was placed to the furnace and exposed for up to 72 ks. In order to retain the scale structure at high temperature, the specimen was then cooled down rapidly to room temperature for metallographic characterization. To determine the oxidation kinetic, the weight change of sample after high temperature oxidation test was measured using electronic balance at time interval of 3.6, 18, 36 and 72 ks. The kinetic of oxidation was evaluated from the weight change per unit surface area of the samples [14] which can be expressed mathematically as:

$$K(t) = \frac{w_t - w_o}{A}$$

where

$K(t)$ = Mass gain or loss after oxidation for t seconds (g/mm^2).
w_t = Mass of sample after oxidation for t seconds (g)
w_o = Initial mass of the sample (g)
A = Initial surface area of the sample (mm^2)
t = Oxidation time

The oxidation kinetic curve was then plotted based on calculated data.

Sample characterization

The X-ray diffraction characterization was carried out using XRD Rigaku SmartLab with CuKα radiation (40 kV, 30 mA). The measurement was conducted at a scan speed of 3 deg/min and scan range of 20-80^o. The phase analysis of the samples before and after oxidation test was performed using Rigaku integrated X-ray powder diffraction software (PDXL) with PDF-4 database.The surface and cross-sectional of the sample after high temperature oxidation test were analyzed by a scanning electron microscope (SEM Hitachi SU3500) at an accelerating voltage of 15 and 20 kV, respectively. The element distribution analysis of oxidized sample was performed by energy dispersive X-ray spectroscopy (EDX Horiba) mapping. For the cross-sectional observation, the oxidized steel was embedded in epoxy resin, cross sectionally cut and polished using various grits of SiC paper for up to a mirror finish (#4000).

RESULTS AND DISCUSSION

Kinetic oxidation of Fe-Cr steel at 1000-1200 K

Figure 1 shows the typical oxidation kinetic curve of Fe-Cr steel after high temperature oxidation at elevated temperatures of 1000, 1100 and 1200 K for up to 72 ks.

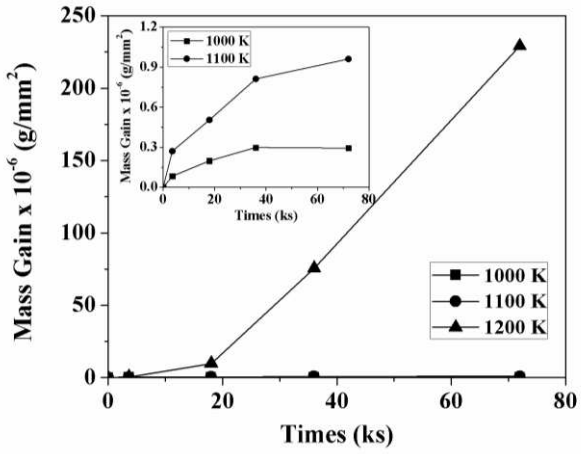

Fig. 1. Oxidation kinetic curve of Fe-Cr steel in air at different temperatures of 1000, 1100 and 1200 K for 72 ks.

The small figure in Fig. 1 represents a magnified image of oxidation kinetic curve of the sample after high temperature oxidation test at

1000 and 1100 K. It can be seen that the oxidation rate is dependent of the oxidation temperature. The mass gain in this study is attributed to the formation of oxide scale on the steel surface. It is obvious from the oxidation kinetic curve that the mass gain of oxidized sample increases with an increase in oxidation time and temperatures. At 1000 K the mass gain of oxidized samples is relatively small increased and almost steady after 36 ks exposure to 0.29×10^{-6} g/mm^2. When the steel is exposed to 1100 K, the mass gain is increased initially and then slows down after 36 ks exposure to 0.96×10^{-6} g/mm^2. A considerable slow mass gain at the aforesaid temperatures suggests that the Fe-Cr steel exhibits an excellent oxidation resistance due to the formation of a protective oxide scale on the steel surface. According to the oxidation kinetic data of the steel after oxidation at 1000 and 1100 K as shown in a small figure in Fig. 2, the oxidation kinetics of Fe-Cr steel on Fig. 1 considerably follow the parabolic plot behavior. In comparison to 1000 and 1100 K, however a very high oxidation rate was observed in the sample after oxidation at 1200 K for 72 ks. Initially, the mass gain of the sample is evidently small, 9.69×10^{-6} g/mm^2 at 18 ks. Nevertheless, after 18 ks exposure, the mass gain of the sample is a sudden change and remarkably increased to 229.09×10^{-6} g/mm^2 at 72 ks obeying linear law (see Figs. 1 and 2). This could be related to breakaway oxidation [6,9], resulting in severe oxidation at higher oxidation temperature.

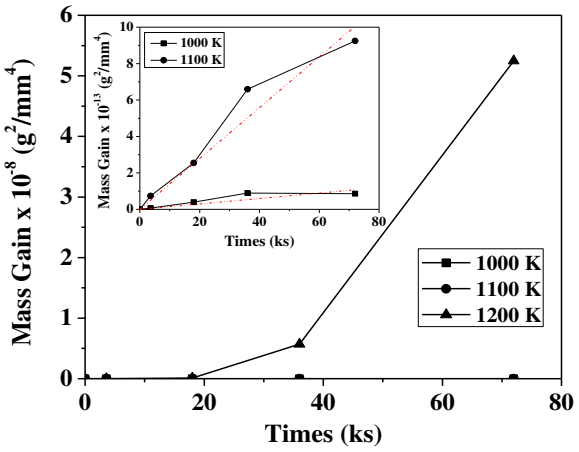

Fig. 2. Parabolic plot of oxidation kinetic data of Fe-Cr steel after oxidation at 1000, 1100 and 1200 K for 72 ks.

Microstructure and phase composition of oxidized Fe-Cr steel

Figure 3 shows the appearances of Fe-Cr steel before and after high temperature oxidation at 1000-1200 K for 72 ks.

Before oxidation as shown in Fig. 3(a), the sample shows a shiny bright surface. However, there is a color change in the sample after high temperature oxidation test. The grey sample surface can be observed after exposure for 72 ks at 1000 K (Fig. 3(b)). With an increase in oxidation temperature, the surface of sample tends to darker (Figs. 3(c) and (d)). This evidence suggests that the formed oxide scales on the alloy surface have a tendency to thicker as the oxidation temperature increases. In addition, from Fig. 3(d) we can see that the cracks are formed on the sample surface after exposure at 1200 K for 72 ks. Generally, the cracks can be formed during high temperature oxidation or cooling period [1,3,8]. The structure of oxide scale will be discussed latter based on phase analysis and microstructure characterization.

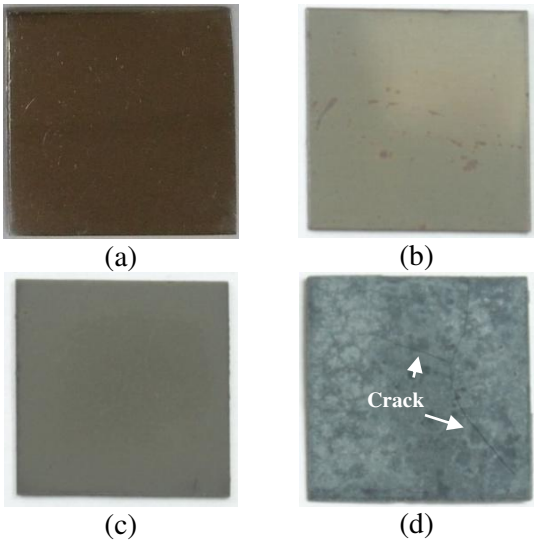

Fig. 3. Appearances of Fe-Cr steel (a) before and after high temperature oxidation test at, (b) 1000 K, (c) 1100 K and (d) 1200 K for 72 ks.

Figure 4 shows the XRD patterns of Fe-Cr steel as received and after high temperature oxidation test at 1000-1200 K for 72 ks, respectively. The XRD analysis reveals that as received (Fig. 4(a)), Fe-Cr steel is composed of ferritic phase. The diffraction peaks of oxidation product are not clearly observed after exposure at 1000 K for 72 ks (Fig. 4(b)). Mainly, the diffraction peak of the substrate was detected by X-ray diffraction with a weak diffraction intensity of Cr-Mn spinel. This is related to a small quantity of oxidation product or a sufficiently thin of formed oxide layer on the steel surface [5], which is closed to the detection limit of XRD. As the oxidation temperature increase to 1100 K (Fig. 4(c)), the diffraction peaks of sample are likely to decrease and the diffraction peak of oxide scales become visible. X-ray diffraction analysis confirms the

formation of $CrMn_{1.5}O_4$ and Cr_2O_3 phases. A difference in oxidation product is found at 1200 K (Fig. 4(d)). The strong peaks of the oxidation product are detected as Fe_2O_3 and $Cr_{1.3}Fe_{0.7}O_3$ phases. Meanwhile, the diffraction peak of the substrate could not be observed attributable to oxide thickening. As results, the X-ray could not reach the steel surface. The aforementioned results reveal that the microstructural development of the oxide scales on the steel surface is affected by oxidation temperature.

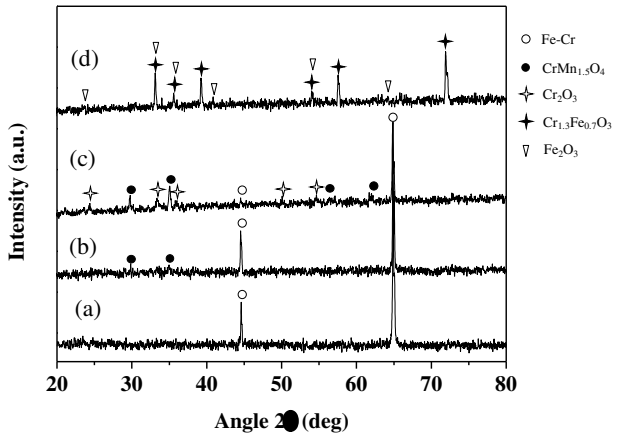

Fig. 4. X-ray diffraction patterns of Fe-Cr steel (a) before and after high temperature oxidation test at different temperatures of (b) 1000 K, (c) 1100 K and (d) 1200 K for 72 ks in air.

Figs. 5(a), (b) and (c) show the surface morphologies of the sample after high temperature oxidation test at 1000, 1100 and 1200 K, respectively for 72 ks. A higher magnification of the surface morphologies of oxidized Fe-Cr steel after oxidation at the aforementioned temperature is presented in Figs. 5(d), (e) and (f).

As shown in Fig. 5(a), the oxide scale developed on the steel surface after exposure for 72 ks at 1000 K is not uniformly distributed. It should be not that a fine grained oxide appears mostly at the grain boundaries (Fig. 5(d)). This implies that grain boundaries become preferential site for oxide nucleation. According to literature study [15] in low-alloy steel, the steel grain size should play an importance role on the diffusion controlled oxidation behavior because in polycrystalline materials, the reactive element is easily to diffuse through the grain boundaries. The result obtained in present study is similar to the previous study that the steel surface is oxidized from grain boundaries to form spinel oxide and Cr_2O_3 phases [16]. The formation of Cr-Mn spinel was due to outward diffusion of Cr and Mn cations and inward diffusion of O anions [4,17].

A much homogeneous surface was observed after oxidation at 1100 K for 72 ks (Figs. 5(b) and (e)). A fine grained oxide is uniformly distributed and covered the entire steel surface. This can be explained due to the fact that the outward diffusion of metal ions and inward diffusion of oxygen ions to form oxide scales enhance at higher temperatures and longer exposure time, resulting the oxide scale growth over the sample. At higher temperature, a difference in surface morphologies of oxide scale is found after oxidation at 1200 K for 72 ks (Figs. 5(c) and (f)). The irregular and porous morphologies can be observed in the outer part of oxide scale after high temperature oxidation. The pores in the oxide layer are mostly formed due to vacancy coalescent which can act as transport paths for oxygen diffusion [1,7,18,19], leading to a high oxidation rate and the formation of thick oxide layer.

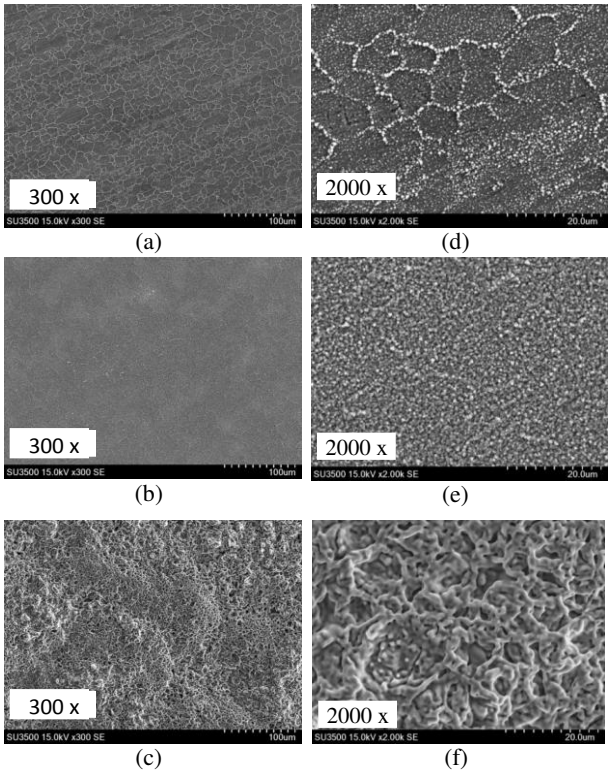

Fig. 5. Surface morphologies of Fe-Cr steel after high temperature oxidation test at ((a), (d)) 1000, ((b), (e)) 1100 and ((c), (f)) 1200 K for 72 ks.

In order to obtain more detail information on the microstructural development of the oxide scale on Fe-Cr steel after high temperature oxidation test at 1000-1200 K for 72 ks, the cross sectional observation was carried out by SEM and the elemental distribution across the oxidized sample was analyzed by EDX. The results are presented in Fig. 6.

The cross sectional images show that the thickness of oxide scale depends on the oxidation temperature. It was increased with increasing oxidation temperature. As can be seen from the SEM image in Fig. 6(a), mostly the formed oxide

scale could not be clearly seen. It can only be seen in certain locations at higher magnification. This result is in good agreement with the results of XRD characterization as shown in Fig 4(b) which show a weak diffraction peak of oxidation product. The reason for this evidence has been explained above. According to the results of EDX elemental mapping as shown in Fig. 6(a), there is a weak

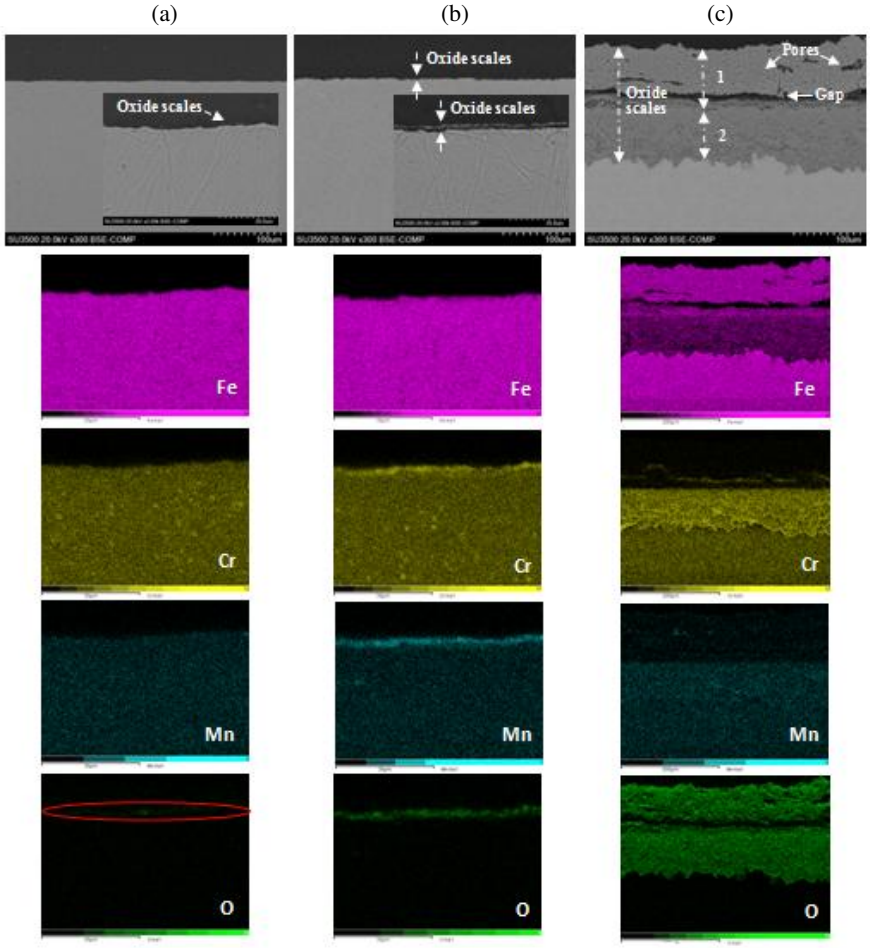

Fig. 6. Cross-sectional images and corresponding EDX elemental map of Fe-Cr steel oxidized at different temperatures of (a) 1000 K, (b) 1100 K and (c) 1200 K for 72 ks in air.

increase in oxygen distribution (red line marker in Fig. 6(a) and trace amount of Cr and Mn on the alloy surface,probably Cr-Mn spinel and/or chromia oxide which was initially formed at the grain boundaries, as shown in the surface morphology characterization of Figs. 5(a) and (d).

As the oxidation temperature increase to 1100 K (Fig. 6(b)), the thin oxide scale with uniform thickness of about 3 µm is observed. According to the results of EDX analysis, the oxide scales are enriched in Cr and Mn. By combining the results of XRD analysis (Fig. 4(c)) and EDX characterization (Fig. 6(b)), the oxide scale seems to be Cr-Mn spinel oxide ($CrMn_{1.5}O_4$) and probably, Cr_2O_3 at the spinel/substrate interface [1,4,11]. The formation of Cr-Mn spinel oxide on the surface of Cr_2O_3 could be related to outward diffusion of Mn through Cr_2O_3 scale. Previous study reported that Mn ions (Mn^{2+}) is easily to diffuse outward through Cr_2O_3 layer among Cr ions (Cr^{3+}) itself [11,17,20] and Fe-ions [11]. The formation of Cr-Mn spinel oxide and Cr_2O_3 scales on the steel surface seems to be effectively acted as oxidation barrier.

At 1200 K (Fig. 6(c)), it is obvious that the scale thickness increases significantly, indicating that the oxide scale is loss in protectiveness. A double oxide layers consisting of porous Fe-rich oxides in the outer layer with oxide thickness of around 80 µm and Fe-Cr oxides in the inner layer with the oxide thickness of around 100 µm can be distinguished clearly from the SEM-EDX mapping result. In accordance to the results of XRD analysis, the oxide layer is composed of Fe_2O_3 and $Cr_{1.3}Fe_{0.7}O_3$. The formation of thick oxide scale could be related to the transition from a protective chromia oxide to poorly protective Fe-rich oxide scale [9,10,13] due to Cr depletion on the steel surface. According to literature [21], at low temperature, the Cr_2O_3 provides a high protection to

oxidation. At high temperatures, the chromia layer starts to transform into a spinel type oxide M_3O_4 (M = [Cr, Fe]). During scale growth, it becomes progressively richer in iron, up to the transformation in hematite (Fe_2O_3). The growth of outer and inner layer is then controlled by outward diffusion of iron and inward diffusion of oxygen, respectively [19]. In addition, from the SEM cross-sectional observation as shown in Fig. 6(c), the Fe-Cr oxides on the steel surface is adherent to the steel substrate without any pores at the oxide/substrate interface. But, pores and gap are appeared in the Fe-rich oxides and at the Fe-rich oxides/Fe-Cr oxides interface. The defects on the oxide layer as void and pore are usually formed due to vacancy accumulation. It can acts as short circuit part of oxygen. Accordingly, oxygen can diffuse easily to the alloy surface [1,7,18,19]. Meanwhile, the reason for gap formation at the inner/outer oxides interface seems to be the same as oxide cracking and spallation which commonly takes place at the oxide/alloy and oxide/coating interface. Several studies have pointed out that oxide cracking and spallation can occur due to thermal stress arising from a different in thermal expansion between oxide and the underlying materials [3,5-8,11,19], grow stress [3,7,8,18] and the formation of other nonadhesive oxide/spinel [7]. During heating and cooling, the thermal stress can enhance the oxide crackingand spalling.

In summary, the cross-sectional observation as presented above corroborates the oxidation kinetic curve as presented in Fig. 1. It was generally accepted that the mass gain has a strong correlation to the thickness of oxide scale. The formation of a thin oxide layer can lead to a small mass gain, associated to that the steel exhibits an excellent oxidation resistance. On the contrary, the formation of thick oxide layer can result in a high mass gain which shows that the steel is susceptible to oxidation.

CONCLUSION

The high temperature oxidation resistance of Fe-Cr steel was studied in air at elevated temperatures of 1000, 1100 and 1200 K for 72 ks. The scale structure formed on the surface of Fe-Cr steel was depended on the oxidation temperature. At 1000 and 1100 K, the Fe-Cr steel exhibits an excellent oxidation resistance attributed to the formation of Cr-Mn spinel oxide and chromia. As oxidation temperature increase to 1200 K, the steel is susceptible to oxidation due to breakaway oxidation by forming Fe-rich oxides in the outer layer and Fe-Cr oxides at the outer layer/substrate interface.

ACKNOWLEDGMENT

This work was supported by Ministry Research, Technology and Higher Education (Insentif Riset Sinas) and Indonesian Institute of Sciences.The authors would like to thank Research Center for Physics–LIPI for providing the characterization facilities.

REFERENCES

1. S. Birosca, G.D. West and R.L. Higginson, Metal **24** (26.5) (2005) 1. http://metal2014.tanger.cz/files/proceedings/metal_05/papers/16.pdf.
2. X. Yu, Z. Jiang, J. Zhao *et al*., ISIJ Int. **55** (2015) 278. http://dx.doi.org/10.2355/isijinternational.55.278.
3. L.W. Pinder, K. Dawson, G.J. Tatlock *et al*., Reference Module in Materials Science and Materials Engineering (2017) 1. http://dx.doi.org/10.1016/B978-0-12-803581-8.10308-X.
4. B. Nikrooz, M. Zandrahimi and H. Ebrahimifar, J. Sol-Gel Sci. Technol. **63** (2012) 286. http://dx.doi.org/10.1007/s10971-012-2786-7.
5. M. Zandrahimi, J. Vatandoost and H. Ebrahimifar, JMEPEG **21** (2012) 2074. http://dx.doi.org/10.1007/s11665-012-0135-1.
6. I. Saeki, Y. Sugiyama, S. Hayashi *et al*., Corros. Sci. **55** (2012) 219. http://dx.doi.org/10.1016/j.corsci.2011.10.018.
7. F.J. Pérez, M.J. Cristóbal and M.P. Hierro, Oxid. Met. **55** (2001) 165. http://dx.doi.org/10.1023/A:1010337530502.
8. J. Yuan, W. Wang, H. Zhang *et al*., Corros. Sci. **109** (2016) 36. http://dx.doi.org/10.1016/j.corsci.2016.03.021.
9. X. Cheng, Z. Jiang, B.J. Monaghan *et al*., Corros. Sci. **108** (2016) 11. http://dx.doi.org/10.1016/j.corsci.2016.02.042.
10. T. Gheno, D. Monceau and D.J. Young, Corros. Sci. **77** (2013) 246. http://dx.doi.org/10.1016/j.corsci.2013.08.008.
11. A.M. Dayaghi, M. Askari and P. Gannon, Surf. Coat. Technol. **206** (2012) 3495. http://dx.doi.org/10.1016/j.surfcoat.2012.02.023.

12. D.J. Young, A. Chyrkin, J. He *et al*., Oxid. Met. **79** (2013) 405. http://dx.doi.org/10.1007/s11085-013-9364-4.

13. H.H. Zhang and C.L. Zeng, J. Power Sources **252** (2014) 122. http://dx.doi.org/10.1016/j.jpowsour.2013.12.007.

14. C.A.C. Sequeira, *High-Temperature Oxidation-Testing And Evaluation*, in: Uhlig's Corrosion Handbook 3rd ed., R.W. Revie (Ed.), John Wiley & Sons, Inc., Hoboken, New Jersey (2011) 1053.

15. V.B. Trindade, R. Borin, B.Z. Hanjari *et al*., Mat. Res. **8** (2005) 365. http://dx.doi.org/10.1590/S1516-14392005000400002.

16. T. Horita, K. Yamaji, Y. Xiong *et al*., Solid State Ionics **175** (2004) 157. http://dx.doi.org/10.1016/j.ssi.2004.09.045.

17. L.F. Liu, S.S. Wu, Y. Chen *et al*., Trans. Nonferrous Met. Soc. China **26** (2016) 1163. https://dx.doi.org/10.1016/S1003-6326(16)64215-2.

18. N.Q. Zhang, Z.L. Zhu, H. Xu *et al*., Corros. Sci. **103** (2016) 124. http://dx.doi.org/10.1016/j.corsci.2015.10.017.

19. Z. Zhu, H. Xu, D. Jiang *et at*., J. Supercrit. Fluids **108** (2016) 56. http://dx.doi.org/10.1016/j.supflu.2015.10.017.

20. K.H. Jo, J.H. Kim, K.M. Kim *et al*., Int. J. Hydrogen Energy **40** (2015) 9523. http://dx.doi.org/10.1016/j.ijhydene.2015.05.125.

21. D. Lussana, D. Baldissin, M. Massazza *et al*., Oxid. Met. **81** (2014) 515. http://dx.doi.org/10.1007/s11085-013-9465-0.